OPEN ACCESS
IOP Publishing | International Atomic Energy Agency
Nuclear Fusion
Nucl. Fusion **57** (2017) 102022 (11pp)
https://doi.org/10.1088/1741-4326/aa7691

3D effects on transport and plasma control in the TJ-II stellarator

F. Castejón[1,4], D. Alegre[1], A. Alonso[1], J. Alonso[1], E. Ascasíbar[1], A. Baciero[1], A. de Bustos[7], D. Baiao[2], J.M. Barcala[1], E. Blanco[1], M. Borchardt[3], J. Botija[1], S. Cabrera[1], E. de la Cal[1], I. Calvo[1], A. Cappa[1], R. Carrasco[1], R. Castro[1], A. De Castro[1], G. Catalán[1], A.A. Chmyga[5], M. Chamorro[1], A. Dinklage[3], L. Eliseev[6], T. Estrada[1], F. Fernández-Marina[1], J.M. Fontdecaba[1], L. García[7], I. García-Cortés[1], R. García-Gómez[1], J.M. García-Regaña[1], J. Guasp[1], R. Hatzky[8], J. Hernanz[1], J. Hernández[1], J. Herranz[1], C. Hidalgo[1], E. Hollmann[9], A. Jiménez-Denche[1], I. Kirpitchev[1], R. Kleiber[3], A.D. Komarov[5], A.S. Kozachoek[5], L. Krupnik[5], F. Lapayese[1], M. Liniers[1], B. Liu[1,7], D. López-Bruna[1], A. López-Fraguas[1], B. López-Miranda[1], J. López-Razola[1], U. Losada[1], E. de la Luna[1], A. Martín de Aguilera[1], F. Martín-Díaz[1], M. Martínez[7], G. Martín-Gómez[1], F. Martín-Hernández[1], A.B. Martín-Rojo[1], J. Martínez-Fernández[1], K.J. McCarthy[1], F. Medina[1], M. Medrano[1], L. Melón[1], A.V. Melnikov[6,15], P. Méndez[1], R. Merino[1], F.J. Miguel[1], B. van Milligen[1], A. Molinero[1], B. Momo[14], P. Monreal[1], R. Moreno[1], M. Navarro[1], Y. Narushima[12], I.S. Nedzelskiy[2], M.A. Ochando[1], J. Olivares[1], E. Oyarzábal[1], J.L. de Pablos[1], L. Pacios[1], N. Panadero[1], I. Pastor[1], M.A. Pedrosa[1], A. de la Peña[1], A. Pereira[1], A. Petrov[5], S. Petrov[10], A.B. Portas[1], E. Poveda[1], G.A. Rattá[1], E. Rincón[1], L. Ríos[1], C. Rodríguez[1], B. Rojo[1], A. Ros[1], J. Sánchez[1], M. Sánchez[1], E. Sánchez[1], E. Sánchez-Sarabia[1], K. Sarksian[11], S. Satake[12], J.A. Sebastián[1], C. Silva[1], E.R. Solano[1], A. Soleto[1], B.J. Sun[1], F.L. Tabarés[1], D. Tafalla[1], S. Tallents, A. Tolkachev[1], J. Vega[1], G. Velasco[1], J.L. Velasco[1], G. Wolfers[1], M. Yokoyama[12] and B. Zurro[1]

[1] Laboratorio Nacional de Fusión, CIEMAT, Madrid, Spain
[2] Instituto de Plasmas e Fusao Nuclear, IST, Lisbon, Portugal
[3] Max-Planck-Institut für Plasmaphysik, Greifswald, Germany
[4] Instituto de Biocomputación y Física de Sistemas Complejos, Zaragoza, Spain
[5] Institute of Plasma Physics, NSC KIPT, 310108 Kharkov, Ukraine
[6] National Research Centre 'Kurchatov Institute', Moscow, Russian Federation
[7] Universidad Carlos III, Madrid, Spain
[8] Max-Planck-Institut für Plasmaphysik, EURATOM-Association, Garching, Germany
[9] University of California-San Diego, San Diego, CA, United States of America
[10] A.F. Ioffe Physical Technical Institute, St Petersburg, Russian Federation
[11] General Physics Institute, Russian Academy of Sciences, Moscow, Russian Federation
[12] National Institute for Fusion Science, Toki, Japan
[13] Instituto Tecnológico de Costa Rica, Cartago, Costa Rica
[14] Consorzio RFX, Corso Stati Uniti 4, 35127 Padova, Italy
[15] National Research Nuclear University MEPhI, 115409 Moscow, Russian Federation

E-mail: francisco.castejon@ciemat.es

Received 15 December 2016, revised 8 May 2017
Accepted for publication 2 June 2017
Published 9 August 2017

Abstract

The effects of 3D geometry are explored in TJ-II from two relevant points of view: neoclassical transport and modification of stability and dispersion relation of waves. Particle fuelling and impurity transport are studied considering the 3D transport properties, paying attention to both neoclassical transport and other possible mechanisms. The effects of the 3D magnetic topology on stability, confinement and Alfvén Eigenmodes properties are also explored, showing the possibility of controlling Alfvén modes by modifying the configuration; the onset of modes similar to geodesic acoustic modes are driven by fast electrons or fast ions; and the weak effect of magnetic well on confinement. Finally, we show innovative power exhaust scenarios using liquid metals.

Keywords: confinement, 3D systems, fuelling, impurity transport, fast particles, stability

(Some figures may appear in colour only in the online journal)

1. Introduction

Stellarator devices are well suited to study the relation between 3D magnetic topology, electric fields and transport. This is a relevant topic not only for stellarators, which are inherently 3D devices, but also for reverse field pinches and tokamaks, where the axisymmetry can be broken due to the introduction of resonant magnetic perturbations [1] or because of the insert of test blanket modules between the coils (see e.g. [2]). The break of axisymmetry implies the enhancement of neoclassical (NC) transport (see e.g. [3] and references therein), with the subsequent onset of an ambipolar electric field, and the strong modification of the dispersion relation of waves in the plasma in comparison with the axisymmetric case. This paper is devoted to exploring the effect of 3D geometry on plasma transport and stability, taking advantage of the TJ-II flexible configuration. Here, the reported results are of key importance and applicable to the new Helias stellarator Wendelstein 7-X (W7-X), in operation since November 2015 [4], see [5] for instance.

The TJ-II heliac is a four period stellarator with helical magnetic axis and with a bean shaped plasma [6]. Changing the currents that circulate by the coils allows us to modify the magnetic configuration shot to shot, or even dynamically in a discharge [7]. Moderated OH and electron cyclotron driven currents can also be used to change the rotational transform profile in a discharge. Recent improvements in TJ-II plasma diagnostics, including the operation of a dual heavy ion beam probe (HIBP), a pellet injection system and liquid Li and LiSn limiters (LLL), have allowed us to get a better understanding of plasma confinement properties. The duplication of the HIBP system permits the measurements in two distant toroidal planes separated by 90°, opening the exploration of asymmetries in electrostatic potential [8] and the search for long range correlation in relevant plasma magnitudes like electric fields [9], which is a foot print of zonal flows (ZFs) [10]. The pellet injector enables the research on core plasma fuelling as well as the exploration of transport and topology properties. The LLL is basic for performing wall coating experiments.

The heating systems for our plasmas consist of two gyrotrons delivering 300 kW each, at X mode with frequencies of 53.2 GHz, i.e. at second harmonic, plus two neutral beam injectors (NBI), which launch co- and counter-beams with 700 kW port-through power at about 33 kV. Although TJ-II plasmas are usually created by electron cyclotron resonance heating (ECRH) [11], direct generation of NBI plasmas in TJ-II under lithium coated walls has been obtained without the help of any other external power supply, as will be shown below.

The reminder of this paper is organised as follows. Section 2 is devoted to the study of impurity transport; section 3 considers the plasma fuelling properties in TJ-II; section 4 shows innovative power exhaust scenarios. The stability properties are revised in section 5; section 6 deals with flow properties in 3D geometries and section 7 studies the Alfvén mode properties. Conclusions are extracted in section 8.

2. Improving confidence in impurity transport predictions: plasma potential asymmetries and physics of empirical actuators

Impurity accumulation is a key open issue in thermonuclear fusion plasmas, particularly in stellarators and in more general 3D geometries, because the NC transport causes inward impurity transport in high-density plasmas, since those plasmas are in the neoclassical ion-root with a radially inwards electric field that tends to confine impurities. This accumulation would cause strong radiation losses, which would jeopardise the performance of an eventual stellarator fusion reactor. Nevertheless, impurity accumulation is known to be absent in some experimental scenarios and devices where the standard theory predicts accumulation, namely, the impurity hole regime in LHD [12] and the high density H (HDH) mode in Wendelstein 7-AS [13]. This motivates the research on these regimes and on the mechanisms to prevent impurity accumulation. An inter-machine study of impurity transport has been conducted [14] using data from impurity hole LHD plasmas and TJ-II low density NBI scenarios, and documented discharges available at the International Stellarator/Heliotron Database (ISHDB, http://ishpdb.ipp-hgw.mpg.de/). The goal was to study, with experiments and simulations, the parameter

dependence of the thermodynamical forces that drive impurity transport in the low-collisionality regime of a helical device with $T_i \approx T_e$. These plasmas present small and negative radial electric fields, so that the inward impurity pinch associated to E_r is close to be balanced by that related to the temperature gradient, in the outwards direction. As a consequence of this, the total inwards impurity pinch is relatively small, although there is no temperature screening, therefore turbulent fluxes or additional neoclassical fluxes associated to potential variations on a flux surface, as discussed below, can easily overcome the small inward impurity pinch and reduce the impurity content of the plasma.

As already noted, the NC theory predicts that in 3D geometries a variation of the neoclassical electric potential on the flux surface, Φ_1, arises (see e.g. [15, 16]). Recently, the first order asymmetric potential Φ_1 is calculated in the $\sqrt{\nu}$ and superbabana-plateau collisionality regimes and, in particular, it is discovered a sub-regime in the superbabana-plateau one, in which this asymmetric term is very large [17]. Φ_1 is usually neglected on the basis of its low impact in the bulk species , but it can matter for impurity transport. NC calculations predict that the asymmetries of the neoclassical electric potential on the flux surface, Φ_1, do have impact on impurity transport. Thus, taking into account the short length scale turbulent electrostatic potential or its long wave-length variation on the flux surface, Φ_1, which is usually neglected in the standard neoclassical approach, might shed some light on the experimental findings regarding impurity transport. This part of the neoclassical potential introduces trapping and radial transport mechanisms that, despite the weak impact on the bulk plasma species, can considerably affect the radial transport of impurities, given their larger charge state. In fact, the spectrum of Φ_1 and its coupling with the distribution function of the impurities as well as the resulting transport level is highly sensitive to the parameters considered. A comparison across devices (TJ-II, W7-X and LHD) has been performed for typical plasma parameters for each device [18]. Figure 1(left) shows the maximum variation of Φ_1 for these three stellarators as a function of the normalized bulk ion collisionality. For the details on these simulations and the specific profiles considered in each case and their corresponding labels (A.I, A.II, etc), we refer the reader to [18]. In particular, the comparison concludes that the impact of Φ_1 on impurity radial particle transport in LHD is strong and can result both in mitigated accumulation at some radial positions and enhanced accumulation at other positions. Interestingly, this feature is shown in figure 1 (right) for a LHD case with plasma parameters comparable to LHD impurity hole plasmas [19]. On the contrary, similar calculations show that Φ_1 is expected to be considerably smaller in W7-X and the transport of C^{6+} is not affected up to an appreciable extent. The potential shows a moderate impact on impurity transport in TJ-II, despite the large amplitude of Φ_1 for the parameters considered. We recognise the need of a more exhaustive and systematic scan and search for scalings of wider applicability, in order to identify a parameter window where Φ_1 reduces the inward impurity flow, as observed at the inner position of LHD. Regarding TJ-II, Φ_1 is found to be the largest compared to the other devices at similar collisionalities, which supports the suitability of TJ-II for the measurement of Φ_1 and the study of its impact on the impurity behaviour. In fact, the study of impurity transport in TJ-II reveals asymmetries in the impurity concentration on a magnetic surface [20].

Experimental studies with Langmuir probes searching for potential asymmetries have thrown direct observations of electrostatic potential variations within the same magnetic flux surface [21], allowing the comparisons of potential asymmetries with the above mentioned NC models. Significant asymmetries are observed in electron-root wave-heated plasmas, which are reduced in ion-root beam-heated conditions and when the electron temperature decreases. The level of the observed electrostatic potential asymmetries is of tens of volts, which is well reproduced by NC Monte Carlo calculations, as it is the dependence of asymmetries on the radial electric field.

Significant progress has been made regarding the understanding of empirical actuators to avoid core impurity accumulation. Here we check the effect of ECRH on the radial electric field on NBI plasmas using the HIBP system that allows one to obtain two radial electric field profiles at two different toroidal positions, showing that the field is less negative when ECRH is switched on, thus reducing the impurity flux. In addition, the investigation has been extended from the plasma edge to the core using the unique capability of the two toroidally separated HIBP diagnostic systems. The mentioned experiments with combined NBI and ECR heating have also shown evidence of the effect of ECRH on turbulence, increasing the level of fluctuations, when ECRH is on, and the amplitude of long-range-correlations (LRC) for potential fluctuations, but not for density and poloidal magnetic fluctuations. The measurements of figure 2 are obtained by fixing one of the HIBP systems at $\rho = 0.6$ and scanning radius with the other one, finding the maximum correlation in potential at that position in ECRH and ECRH + NBI plasmas. Whereas ECRH influences the level of fluctuations in a wide range of plasma densities, ECRH-induced reversal of the NC radial electric field has been observed only in low-density plasmas [22].

3. Plasma fuelling experiments and neutrals dynamics

Core density control is a critical issue on the path towards the development of steady-state scenarios in 3D magnetically confined plasmas, especially for the HELIAS line [23]. Therefore, an accurate and precise estimate of core particle transport and core fuelling is of critical interest in order to assess the risk of potential core depletion in large stellarators. This interest has triggered a set of inter-machine comparative pellet fuelling studies [24, 25] whose goal is to achieve a detailed understanding of pellet ablation mechanisms and subsequent particle transport. First core plasma fuelling experiments, using a cryogenic pellet injector system and associated diagnostics have been performed in the TJ-II stellarator, which has enabled particle fuelling and transport experiments in this device [26].

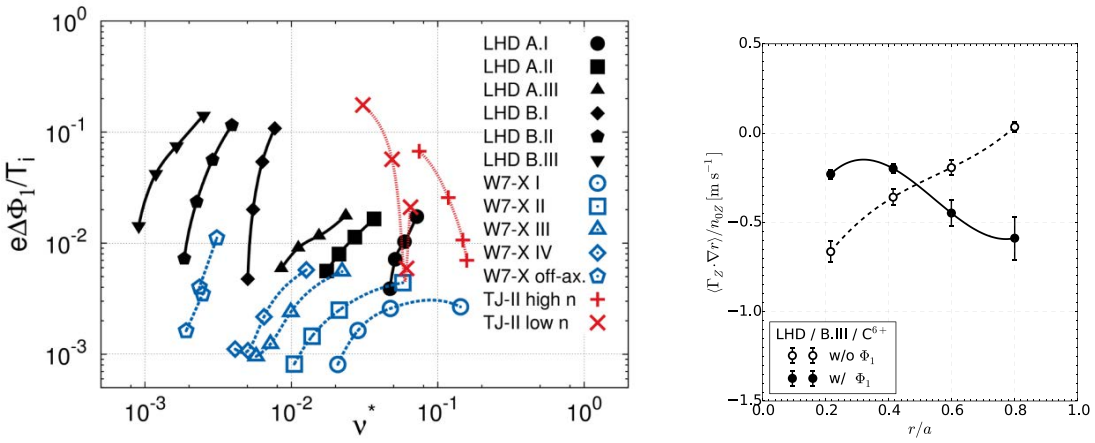

Figure 1. (left) Ratio $e\Delta\Phi_1/T_i$ as a function of the normalized collision frequency for different positions and profile sets (each corresponding to a set of points linked by a line). Here, e is the electron charge, T_i the bulk ion temperature and $\Delta\Phi_1$ the maximum potential variation on a surface. (right) Radial particle flux of C^{6+} in LHD normalized to the density with and without Φ_1.

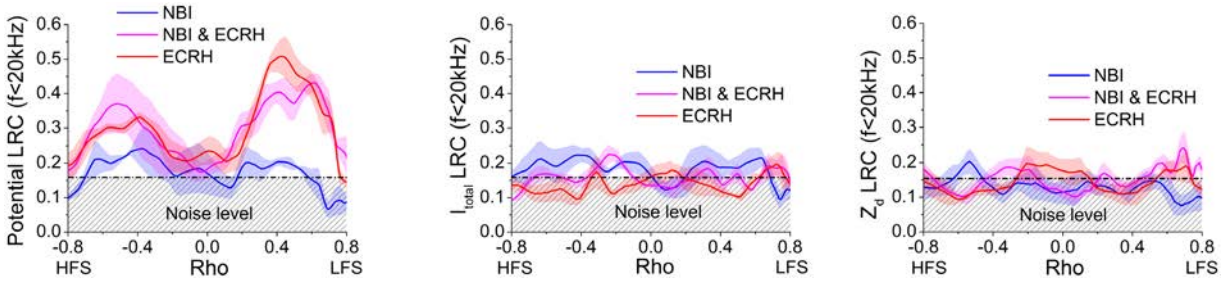

Figure 2. Long range correlation (LRC) of potential (left), total current, proportional to density (centre), and poloidal magnetic field (right). One of the HIBP systems is fixed at $\rho = 0.6$, while the other is scanned radially.

We have studied scenarios representative of difficult central fuelling and of loss of density control in NBI plasmas, in which the density (including the core) is reduced by means of gas puff control. A small pellet is injected at an intermediate radial position and density evolution is measured with Thomson Scattering and interferometry. In particular, a density increase due to ablation is initially observed outside the core ($\rho \approx 0.5$), moving inwards and reducing with time. Finally, we observe a core density increase after the complete ablation of the pellet. This transient particle transport has been successfully described using NC simulations with DKES code (see figures 3 and 4), and therefore could be extensible to other helical devices. Concluding that pellets that do not reach the magnetic axis may still be able to mitigate core density depletion would be a very relevant result in view of density control in reactor-size helical devices, where the penetration depth of the pellet may not be large enough to reach the core for high densities.

Beyond fuelling studies, pellet injection has been used also to perturb the plasma equilibrium potential and to study the subsequent relaxation. A sudden perturbation of the plasma equilibrium is induced by the injection of a cryogenic hydrogen pellet in the TJ-II stellarator, followed by a damped oscillation in the electrostatic potential. The waveform of the relaxation is consistent with the gyrokinetic (GK) theory of zonal potential relaxation in a nonaxisymmetric magnetic geometry, of which this would be the first experimental validation [27]. The frequencies and damping rates of these oscillations are consistent with GK simulations of ZF relaxation and semi-analytical calculations of ZF relaxation properties [28] in this magnetic geometry. The importance of these studies relies on the fact that turbulent transport properties of a magnetic confinement configuration are expected to depend on the features of the collisionless damping of ZFs.

Usually, even 3D fuelling simulations assume a cloud distribution of neutrals, given by the puffing characteristics [29]. Here, we explore the possible response of neutrals to plasma turbulence, which could modify fuelling properties. With this aim, the helium line-ratio technique was applied with a spectroscopic high-speed camera set-up looking to the emission of helium puffed close to the separatrix. In this way, we obtain the 2D image of the edge plasma electron density with a few millimetres spatial resolution and exposure times down to 15 μs. This technique allows us to measure the turbulent coherent electron density-structure of blobs that have been compared with the raw helium emission. The differences between plasma density and raw emission structures can give insight on the neutral distribution, provided the rate coefficient for the intensity emission of the lines is known. Figure 5 shows the normalised and de-averaged emission intensity ΔI_{667}^{N}, (given by $\Delta I_{667}^{N} = (I_{667} - \langle I_{667}\rangle)/\langle I_{667}\rangle$), electron density Δn_e^{N} (where $\Delta n_e^{N} = (n_e - \langle n_e\rangle)/\langle n_e\rangle$), and neutral density Δn_0^{*N} (given by $\Delta n_0^{*N} = (n_0^* - \langle n_0^*\rangle)/\langle n_0^*\rangle$, where $n_0^* = I_{667}/n_e$). It is seen that the quantity Δn_0^{*N} presents a structure that denotes

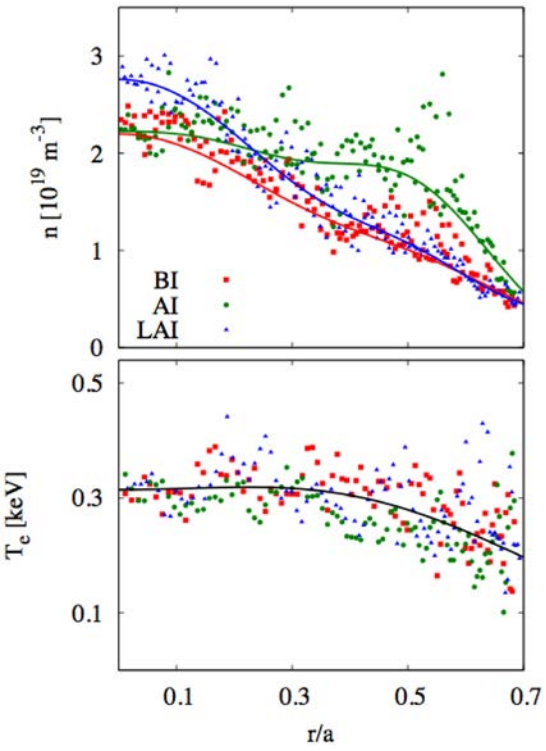

Figure 3. Electron density and temperature profiles before the pellet injection (BI, #39063), immediately after the pellet injection (AI, #39062), and long after the pellet injection (LAI, #39065).

that neutral density is not described just by a diffusion process, but it is influenced by plasma density turbulence.

The conclusion of these measurements points to the fact that the thermal neutrals coming from the puffing valve react to the plasma fluctuations becoming also turbulent at frequencies of 10–100 kHz and with dimensions of one to several centimetres (see figure 5). The responsible mechanism to bring neutrals spatially and temporally inhomogeneous must be the turbulent local electron impact on ionization by the plasma blobs and holes [30]. This can substantially modify the fuelling properties and these results open an almost fully unexplored area of research.

Another key topic for fuelling is whether anomalous transport driven at the plasma edge influences the scrape-off layer (SOL) width. We have performed experiments in the TJ-II stellarator and have found that the SOL density profile is affected by the structure of edge radial electric fields and fluctuations. It is concluded that SOL profiles are coupled with edge plasma parameters and consequently optimizing SOL power exhaust conditions requires considering transport in the edge region.

4. Innovative power exhaust scenarios using liquid metals

Beyond developing techniques and empirical actuators to reduce impurity accumulation, it is mandatory to reduce the impurity influx from the walls in magnetic confinement devices. To do that, novel solutions for plasma facing components based on the use of liquid metals like Li and SnLi alloys have been developed. The TJ-II program on liquid metals,

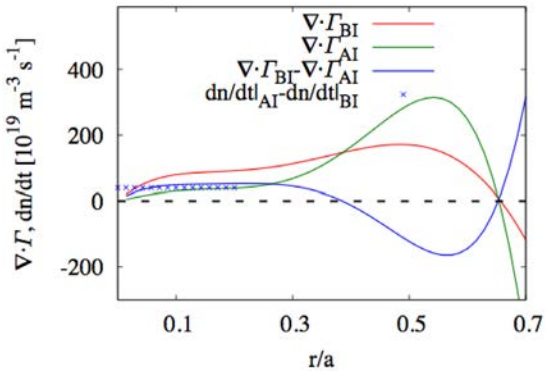

Figure 4. Contribution of neoclassical transport, calculated with DKES, to the particle balance equation in NBI plasmas, and comparison with the experiment.

presently leading in the stellarator community, addresses fundamental issues like the tritium inventory control or the self-screening effect of liquid Li driven by evaporation to protect plasma-facing components against huge heat loads, using recently installed Li and SnLi liquid limiters. Biasing of LLL with respect to carbon ones has evidenced the important role of the secondary electron emission of plasma-exposed surfaces in the development of enhanced confinement modes. Very recently, LiSn alloys have been exposed to TJ-II plasmas in a capillary porous system (CPS) arrangement. The main results are [31]:

- H retention values of ~0.01% H/(Sn + Li) at $T < 450$ °C were deduced from thermal desorption spectroscopy (TDS) at the laboratory, in agreement with previous reports and *in situ* TDS in TJ-II. This is relevant to diminish T-retention in next step devices.
- Insertion of a solid LiSn sample into the edge of TJ-II does not cause any significant perturbation of the plasma parameters. The evolution of $Z_{\rm eff}$ during the discharge shows that the influx of impurities in the plasma is very small, as can be seen in figure 6. $Z_{\rm eff}$ values typically below 1.5 and very low $P_{\rm rad}/P_{\rm in}$ values (<2%) were deduced for cold LiSn sample. Even in the worst case, corresponding to hot sample, the largest value of $Z_{\rm eff}$ is kept below 1.8, thus producing clean plasmas.
- Conversely, plasma operation became impossible if the alloy is directly deposited on the stainless steel support without mesh.
- Only Li emission was detected. No traces of Sn were detected by visible and UV spectroscopy.
- H recycling did not evolve with temperature.
- Poor thermal conductivity of the CPS of LiSn was deduced for a damaged stainless steel mesh.

These results provide good perspectives for use of LiSn alloys as a PFC in a fusion reactor.

As a further example of the beneficial effect of Li coating, we achieved plasma start-up in TJ-II under Li-coated walls using only NBI, without the help of any other external power supply, although with large plasma current and the presence of a high energy electron population. This has been achieved despite the large shine through in the phase of plasma creation

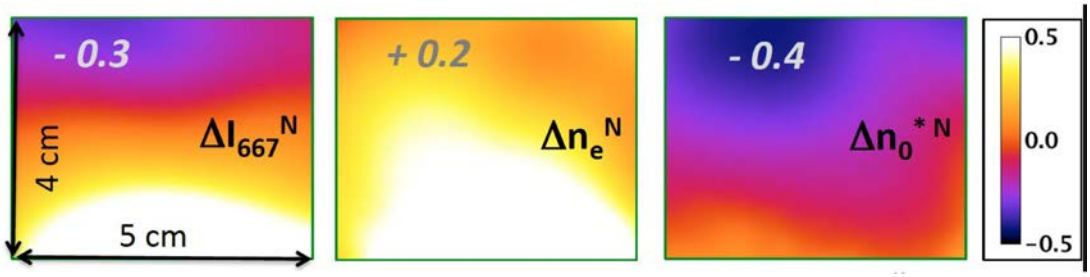

Figure 5. (From left to right) Normalised and de-averaged emission intensity ΔI_{667}^{N}, electron density Δn_e^{N} and neutral density Δn_0^{*N}.

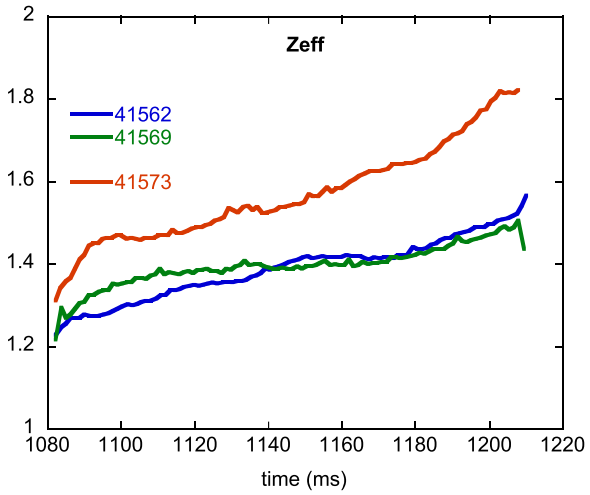

Figure 6. Time evolution of $Z_{\rm eff}$ during three reference shots deduced from soft x-ray (SXR) traces. Discharges 41562 and 41569 correspond to experiments with limiter, while the limiter was heated in the shot number 41573.

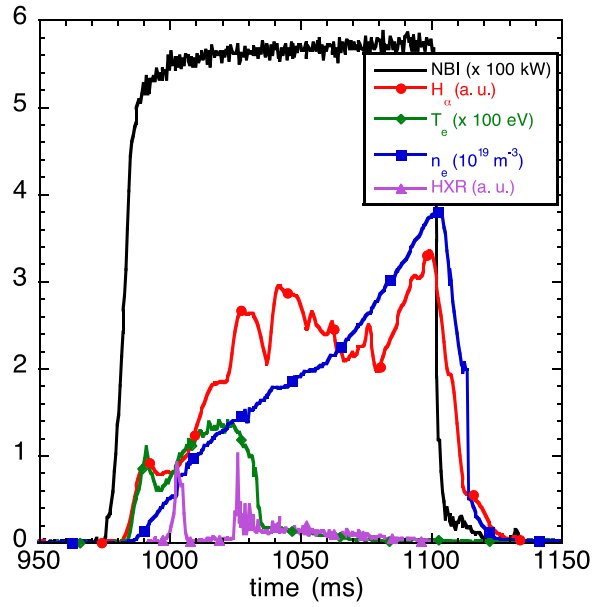

Figure 7. Time traces of the NBI start up with full conditioned walls. The NBI power, H_α emission, central electron temperature measured by ECE, line density and hard x-ray evolution can be seen.

[32]. An example of the time traces is shown in figure 7, where it can be seen that the plasma breakdown happens about 10 ms after the NBI power is switched on. Hot plasma is produced during the NBI pulse and the ECE signal falls when the plasma density reaches the cut-off value.

5. Plasma stability studies

Experiments on TJ-II have shown that stability at high beta values is better than predicted by linear stability analyses. One of the possibilities offered by TJ-II flexibility is to change the magnetic well keeping almost the same rotational transform profile. Mercier criterion ensures stable plasmas when the sum of the terms corresponding to magnetic shear, plasma current, geodesic curvature and magnetic well is positive. As the plasma current is negligible [33] and TJ-II is an almost shearless device, the Mercier stability is then a competition between magnetic well and geodesic curvature. It has been shown that a reduction of magnetic well has a direct impact on fluctuations without reducing plasma confinement [34]. In fact, the energy confinement time depends more on NC effects and on the size of the configuration (see figure 8) than on magnetic well. This result shows that Mercier stability calculations are missing some stabilization mechanisms, which could be explained by self-organization processes involving transport and gradients.

The degradation of confinement time with density observed in figure 8 seems to be in contradiction with ISS04 scaling law, which predicts an improvement of confinement with density. But one has to take into account that absorbed power in NBI plasmas increases strongly with density. Considering that the confinement time satisfies $\tau_E \propto n_{\rm e}^{0.54} P^{-0.61}$, one can understand that the final confinement time is finally degraded with density in this particular case.

The effect of the magnetic well scan on electromagnetic modes has also been studied, showing consequences on the properties of the Alfvén Eigenmodes (AEs) spectra, as will be shown in section 7, and the onset of a mode that is a candidate to geodesic acoustic mode (GAM) [35].

GAMs are relevant for confinement, given their interaction with broadband turbulence and fast particles, and they are expected to be strongly damped in TJ-II, because of the large ripple and rotational transform values of this device [10]. The latter reason implies that GAMs must be driven steadily to overcome the damping in order to survive, so a driver must be identified if GAMs are detected. Energetic ions can act as a driver, giving rise to EGAMs [36], which could also be the mode shown in [33].

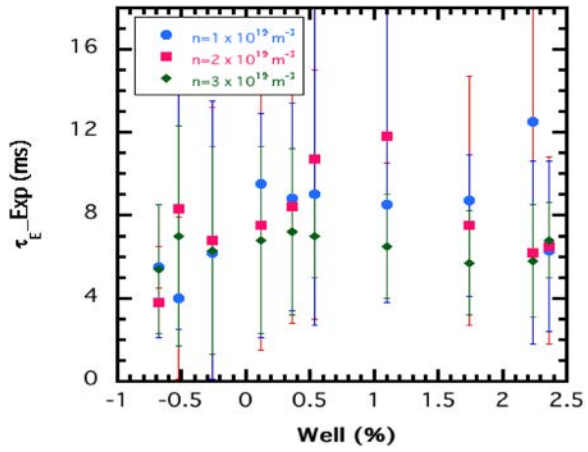

Figure 8. Energy confinement time as a function of magnetic well for three values of the plasma density. Those configurations with negative magnetic well values should be unstable.

It has been demonstrated that fast electrons are acting as a driver for acoustic modes in TJ-II plasmas [37]. During ECRH experiments at low line averaged electron densities, $0.15 < n_e < 0.6 \times 10^{19}$ m^{-3}, radiation signals show intense coherent oscillations ($\delta I/I \sim 5\%$) with frequencies of several tens of kHz (see figure 9, left). Several configurations have been explored and it was determined that the modes: (i) appear at radial positions close to the ones of low-order rational values of the rotational transform (between the effective radius 0.4 and 0.7), (ii) are excited by fast-electron populations [38], and (iii) disappear when the islands rotate. Their frequencies scale with ion sound speed ($f_{ISW} = nC_s/2\pi R$) and the poloidal mode structure of the fundamental harmonic agrees with that of GAMs. Nevertheless, a $n \neq 0$ toroidal structure is deduced from toroidal correlation of equivalent bolometer signals (see figure 9, center): a clear propagation of the mode in the counter-B direction is observed (see figure 9, right). If they are confirmed as EGAM, theoretical studies should consider that the modal structure of GAMs in stellarator geometries is more complex than that in tokamaks. Consequently, the expectations on transport effects should be also revised for these devices.

In order to explore its dependence on the 3D magnetic configuration, the stability of electrostatic modes in TJ-II configurations has been studied by means of global linear GK simulations using the EUTERPE code. Unstable electron-driven modes are found in typical TJ-II plasmas, whose amplitude peaks at very localized spatial regions, determined by both the magnetic field line curvature and the magnetic shear. The electrostatic modes are more unstable for high values of the rotational transform, which is interpreted as a consequence of the interplay between the stabilization by local magnetic shear and the alignment of modes with the magnetic field lines. Given the freedom that stellarators present to design the magnetic configuration, these findings could give a guide to design magnetic configurations that provide linear stability for electron-driven modes. The effect of strong spatial localization of electrostatic unstable modes has also been studied in non-linear ion temperature gradient simulations in TJ-II, showing that, although the nonlinear saturation tends to homogenize fluctuations along the flux surface, some signatures of the localization remain both in the fluctuations spectra and bispectra.

6. Plasma flows and electromagnetic effects

TJ-II has provided clear evidence of the impact of 3D magnetic structures on plasma confinement and L-H transitions. Observations regarding the temporal ordering of limit cycle oscillations (LCO) at the L-I-H transition, linked to the radial propagation of rotation velocity, emphasize the role of plasma turbulence. LCOs are observed close to the L-H threshold in configurations with a low order rational located inward from the ExB shear location [39]. Furthermore, radial electric fields, ZF-like structures, time memory and radial correlations are modulated by low order rationals [40].

We have also performed experiments on the effect of magnetic islands on the plasma perpendicular flow and density turbulence. Doppler reflectometry has been used to study the plasma flow in ohmically induced magnetic configuration scans, which changed the rotational transform profile and the location of the rational values of the rotational transform [41]. A characteristic signature attributed to the 3/2 magnetic island as it crosses the Doppler reflectometer measurement position consists of a modulation in the perpendicular flow that changes twice its direction [42]. The perpendicular flow reverses at the centre of the magnetic island and a flow shear develops at the island boundaries. An example is shown in figure 10, where the 3/2 magnetic island, on its way from the plasma centre to the plasma edge, crosses the Doppler reflectometer measurement region when the net plasma current is near −5 kA (see figures 10(*b*) and (*c*)). Besides, as shown in figures 10(*d*) and (*e*), an increase in the perpendicular flow fluctuation intensity is measured at the outer and inner boundaries of the magnetic island; the increase being more pronounced for low frequencies (below 50 kHz). Synchronous with the increase in the flow fluctuations, a reduction in the density fluctuation level is measured (see figures 10(*f*) and (*g*)). This reduction is more pronounced in the inner boundary of the island, i.e. when the island is overpassing the Doppler reflectometer measurement region, where the flow shear is stronger. These observations could explain the link between magnetic islands and transport barriers in a number of fusion devices.

It is known that the formation of transport barriers in TJ-II is promoted when low order magnetic resonances are placed in the appropriate plasma region. The stability of such barriers is subject to the MHD stability of the corresponding magnetic resonances [43] and a close relationship has been identified between abrupt changes in transport (in the form of transport pulses or the formation of transport barriers), MHD activity and the location of magnetic resonances. Now, applying a novel causality detection technique (the entropy transfer) to quantify the information transfer between magnetic oscillations and locally measured plasma rotation velocity related to ZFs, it is confirmed that magnetic oscillations associated with rational surfaces play an important and active role in

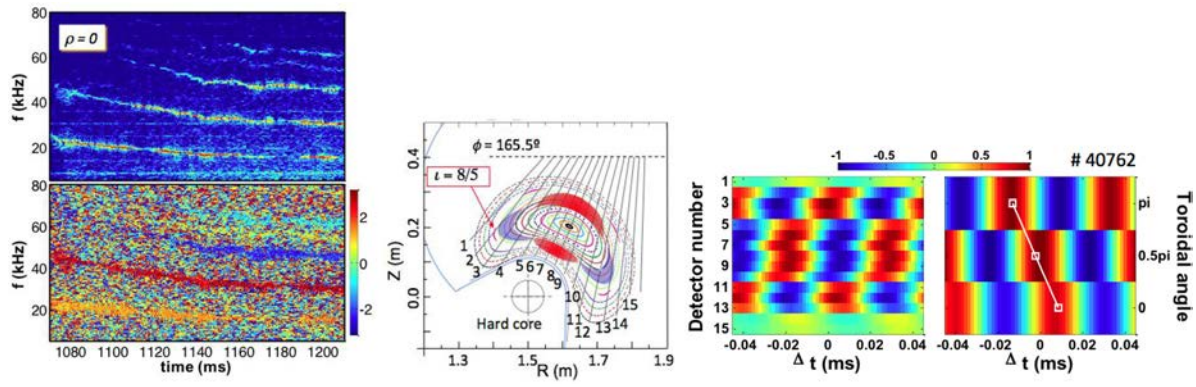

Figure 9. (left) Signals cross-spectrum and cross-phase from two central bolometers separated $\Delta\phi = 90°$. (Centre) Scheme of a 16-channel photodiode array on top of the Poincaré plot of one of the configurations studied. A hypothetical $m = 2$ mode structure, characteristic of standing wave is overplotted. (right) Correlation of bolometer array signals with the reference channel 8 ($\rho = 0$), in the frequency range of the first harmonic. (*a*) Poloidal and (*b*) toroidal correlation. The fitted slope of white line is $d\varphi/dt = -145.6$ rad ms^{-1}.

confinement transitions [44]. For example, in many cases of L-H transition with co-NB heating and fuelling, fast repetition rates (~1 ms^{-1}) of transport barrier breaking and re-establishment are due to the dynamics of rotating magnetic islands: measured ExB island rotation velocity is compatible with L- and H-confinement modes, while hybrid confinement states characterized by repeated barrier formation and breaking processes seem to imply the rotation of the islands with a diamagnetic drift in the ExB frame [45]. These hybrid regimes, different from L- or H- confinement modes, are a consequence of edge-reaching pulsed transport events.

LRC is an indication of the existence of ZFs, which are expected to decrease the turbulence level. Comparative studies in tokamaks and the TJ-II stellarator [46] in hydrogen and deuterium plasmas have shown that there is a systematic increase in the amplitude of LRCs during the transition from H to D dominated plasmas in the tokamaks but not in the TJ-II stellarator, suggesting that ZFs are playing a role on isotopic effect in tokamaks, but not in stellarators. Furthermore, NC radial electric fields are coupled with the amplitude of LRCs providing evidence of the mutual interaction of NC and turbulent mechanisms [47] in qualitative agreement with GK simulations.

7. Physics basis for controlling fast particles: the roles of ECRH and magnetic configuration

The study and control of AEs is a key task in plasma devices, given the impact of these modes on fast ion confinement, which will influence the fusion performance and the efficiency of heating and current drive. Steady and chirping AEs driven by fast ions coming from NBI have been found previously in TJ-II [48]. Here we explore several mechanisms to control and mitigate AEs. The HIBP diagnostic is capable of measuring simultaneously the oscillations of plasma electric potential, density and poloidal magnetic field, and the Mirnov coils can measure the magnetic fluctuations. The mode position is extracted here from the correlation between HIBP and Mirnov coils signals [49].

First of all, ECRH was applied on NBI-heated low density plasmas of TJ-II. A change from steady to chirping frequency or even to a mitigation of the AEs was observed [50], and new

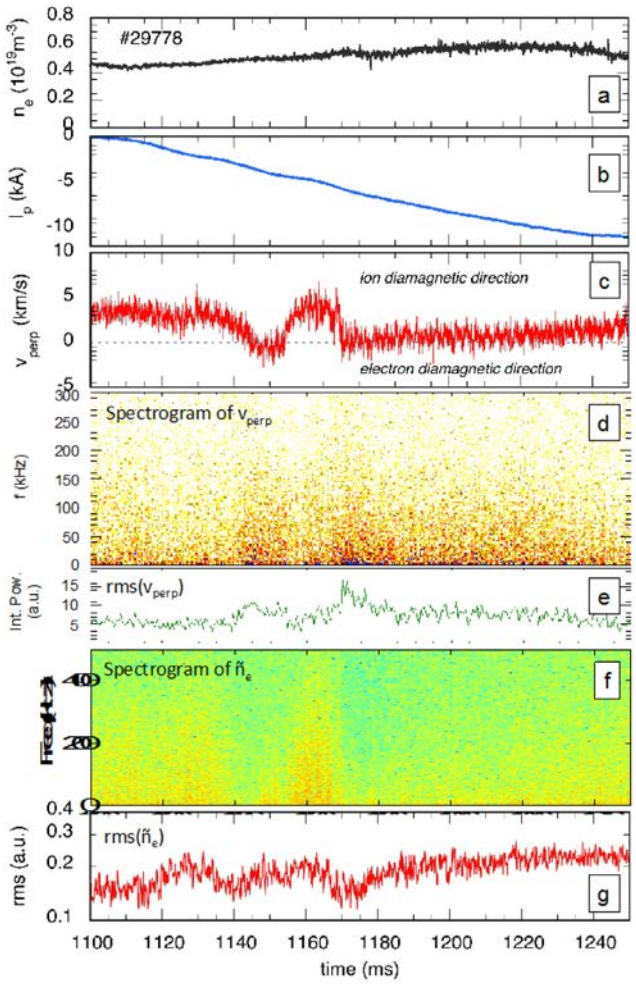

Figure 10. The time evolution of line-averaged density (*a*); net plasma current (*b*); perpendicular flow (*c*); spectrogram (*d*) and root mean square (*e*) of the perpendicular flow fluctuations, and spectrogram (*f*) and rms (*g*) of the density fluctuations.

results show that moderate off-axis ECH power changes the continuous character of the modes significantly, triggering a frequency chirping behaviour. As the ECRH power increases (power scan from 80 to 225 kW), the amplitude of the chirping AE mode increases while the bursts periodicity becomes more regular. A relatively small change of the injection direction of

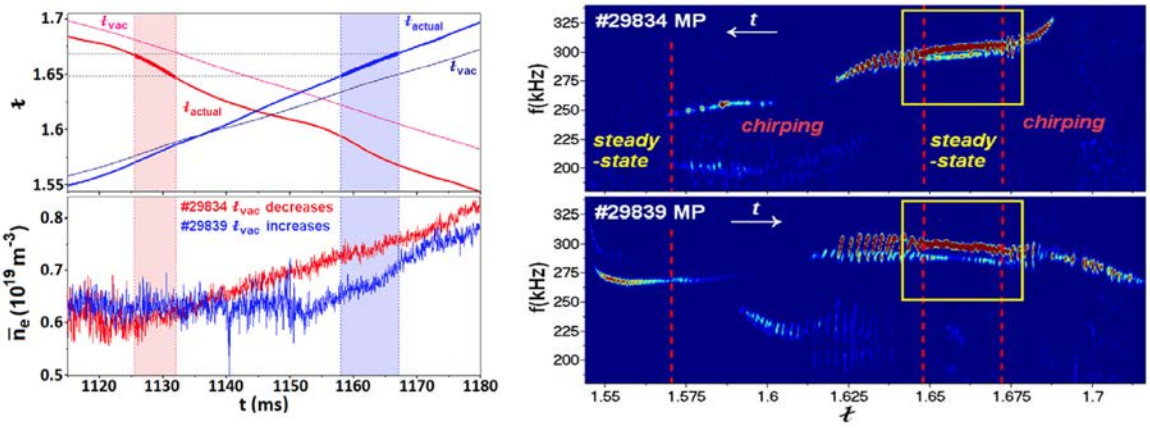

Figure 11. (left) Time traces of the evolution of the vacuum and actual rotational transform and of the density during the configuration scan. The chirping appears always for the same values of rotational transform (marked with stripes), as can be seen on the right panel, where the spectrogram of the modes is plotted as a function of the rotational transform, showing that chirping appear at fixed values of this parameter.

any of the two available ECRH beams modifies the character of the observed AE, from steady to chirping. It still remains to clarify if this change in the chirping/steady nature of the AE is due to plasma profile changes or to the modification of damping by ECRH. HIBP measurements show that the chirping mode has a ballooning structure in plasma potential but a symmetric structure in the poloidal magnetic field B_{pol} [51]. These experiments show that ECRH is a potential tool for AE control in reactor-relevant conditions.

On top of the effect of ECRH, we expect the magnetic configuration to have a strong effect on AEs properties, since the dispersion relation is modified varying the configuration. We take advantage of the above-referred TJ-II flexibility to explore the effect of the magnetic configuration on AEs, which opens new ways to control them and, hence, their effect on fast ion confinement. We have induced Ohmic current in order to vary the rotational transform in TJ-II in a single configuration, which modified strongly the mode properties due to both the change of the wave vector of the mode [52] and the dispersion relation in the plasma. Using the dependence of the parallel wave vector on the mode order and rotational transform value, $k_{\|} \propto \left| n - \frac{m\iota}{2\pi} \right|$, the mode order could be identified. New experiments based on dynamic configuration scans in TJ-II in single discharges have allowed us to explore the change of character of the modes. We used L-mode hydrogen plasmas heated with co-, counter- and balanced NBI and ECRH in various magnetic configurations with rotational transform $\iota(a)/2\pi = 1/q \sim 1.5$–$1.6$. We could observe chirping modes obtained with NBI only in plasmas (without the intervention of ECRH) with densities similar to those of earlier studies (see figure 11). The absence of ECRH in the discharges studied here shows that this is not a necessary ingredient to obtain chirping modes in TJ-II. Using the HIBP diagnostic, we deduce that the location of the AE chirping mode is between $-0.8 < \rho < 0.8$ in these experiments. Chirping modes have a specific spatial structure: the electric potential perturbations have a ballooning character, while the density and B_{pol} perturbations are nearly symmetric for both ECRH + NBI and NBI-only plasmas. In TJ-II, a dominant effect on the non-linear evolution of the AE from chirping to steady frequency state is the magnetic configuration, determined by vacuum ι and plasma current I_{pl} [53].

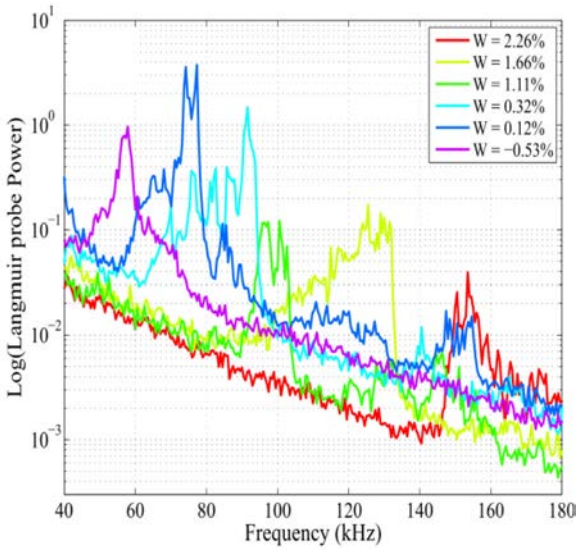

Figure 12. AE frequency spectra for plasma discharges with similar densities performed at configurations with different magnetic well values (it is seen that the maxima of the spectra move to lower frequencies as magnetic well decreases).

The importance of distinguishing chirping from steady behaviour relies on the different effect of the mode on fast ion confinement. We use the fast neutrals flux, measured by the compact neutral particle analyser (CNPA), as a proxy for the fast ion density, so the larger the CNPA flux the larger the fast ion concentration and confinement. Hence, we can compare the fast ion confinement of different experiments by comparing the CNPA spectra, in case that the fast ion source is the same. We use those CNPA measurements averaged in time intervals of 10 ms for almost constant plasma density, to compare the fast ion confinement in those intervals. It is seen that the confinement is better in the cases with chirping and mitigated AE than in the one with steady AE [54].

We have also investigated the influence of magnetic well on AEs properties, taking advantage of the TJ-II flexibility. We have found a strong influence of this parameter on AEs

on frequency, mode number and amplitude [33]. The complexity of AE dispersion relation in TJ-II provokes such strong changes in the mode properties. In particular, it is observed that the frequency of the destabilised modes is decreasing with the magnetic well (see figure 12): the lower the magnetic well the lower the frequency, for similar plasma densities. This allows one to change the population of resonant ions, since it is expected that the energy of the resonant ions is lower in the case of lower AE frequencies. The amplitudes of the modes are found to be non-monotonic with the magnetic well and the nature and order of the modes change from one configuration to another, since the gaps appear at different frequencies and positions of the spectrum. Global and helical AEs (GAEs and HAEs) appear in the deep well configurations and only HAEs happen in the hill cases.

AEs studies are commonly based on equilibrium nested flux surfaces. Nevertheless, magnetic islands can appear close to the rational values of the rotational transform that can modify the AE spectrum and open new gaps in the continuum, since islands are repetitive structures in the plasma. In TJ-II, coherent modes in NBI-heated plasmas at frequencies generally below those of helicity induced AEs ($f < f_{\mathrm{HAE}}$) are explained as GAEs and discrete shear-AEs induced by a non-rotating magnetic island (MIAE). Rotating islands are also found to interact with AEs: if they share the same helicity, they perturb each other; otherwise, new AEs are excited via wave–wave coupling [55].

8. Conclusions

The influence of 3D geometry on confinement physics has been explored taking advantage of the TJ-II characteristics and advanced diagnostics capability. These studies are especially relevant after the starting of Wendelstein 7-X operation. The break of axisymmetry causes that NC transport is not automatically ambipolar, giving rise to the onset of a radial electric field. Impurity transport is also affected and we have explored here the conditions in which the inward impurity pinch is decreased and allow that other transport terms can decrease impurity accumulation. NC theory that includes the effect of variation of the electrostatic potential within the flux surface predicts the existence of asymmetries on the magnetic surfaces, which have been observed experimentally in TJ-II, and can have significant influence on impurity transport, as Monte Carlo calculations predict.

NC calculations predict central plasma density depletion in low collisionality plasmas, which has triggered studies of core fuelling in helical devices. We have shown that this density depletion can be at least partially mitigated by injecting a pellet, even if it is ablated before reaching the plasma centre.

Pellet injection has not been only used as a fuelling tool, but it has allowed us to obtain for the first time a direct observation of the electric field relaxation, in agreement with GK simulations. Another important characteristic of the fuelling in TJ-II is the structure of the neutrals that reflect the blobs found in density turbulence. As the fuelling experiments demonstrate, the plasma wall interaction in TJ-II depends strongly on the 3D geometry and makes TJ-II a well-suited laboratory to explore innovative solutions for plasma facing components based on the use of liquid metals like Li and SnLi alloys. On top of that, NBI-only plasma start up has been achieved in Li-coated walls, despite of the large beam shine-through in TJ-II before plasma is created.

The 3D geometry has also strong effects on plasma stability and turbulence, since the dispersion relation of the waves and the MHD properties will change strongly with the geometry. We have obtained stable plasmas in theoretically Mercier-unstable configurations and have found that the confinement depends rather on NC properties and volume than on Mercier criterion. Firm candidates to EGAMs driven by fast ions and fast electrons are also detected in TJ-II, showing the effect of rational values of the rotational transform on the latter modes, observed for the first time. The toroidal structure of the fast electron driven modes shows $n = 1$, different from $n = 0$ obtained in tokamaks.

MHD stability and the magnetic island onset have a strong influence on momentum transport and on L-H transition. The plasma flow is affected by the magnetic island, as can be directly measured by Doppler reflectometry. The rational values of the rotational transform can give rise to the cyclic formation and destruction of transport barriers, playing a key role in the L-H transitions and provoking hybrid states between L and H mode.

The dispersion relation of AEs is also affected by 3D geometry. In particular, we have shown that the magnetic well is a governing parameter of the frequency of the mode: the larger the well, the higher the frequency, for the same density. The rotational transform plays a key role in the AEs properties: we have found the rotational transform windows in which the mode presents a chirping nature and the ones in which its frequency varies steadily following plasma current and density. The rational values of the rotational transform can give rise to the presence of islands that open new gaps in the continuum of the spectrum, triggering MIAEs. All these mechanisms pose the magnetic configuration as an important tool to control AEs and, hence, fast ion confinement, beyond ECRH. New experiments show that the amplitude of the chirping AE mode increases while the bursts periodicity becomes more regular, as the ECRH power increases.

Acknowledgments

This work has been carried out within the framework of the EUROfusion Consortium and has received funding from the Euratom research and training programme 2014–2018 under grant agreement No 633053. The views and opinions expressed herein do not necessarily reflect those of the European Comission. This work has been also funded by the Spanish Ministerio de Economía y Competitividad under Projects ENE2013-48109-P, ENE2013-48679-R, ENE2014-52174-P, ENE2014-58918-R, ENE2014-56517-R, ENE2014-56517-R, ENE2015-64914-C3-1-R, ENE2015-70142-P. Research and data analysis done by Kurchatov team (chapters 2, 3 and 7) were funded by Russian Science Foundation, Project

14-22-00193. The work of AVM was partly supported by the Competitiveness Program of NRNU MEPhI.

ORCID iDs

F. Castejón https://orcid.org/0000-0002-4654-0542
D. Alegre https://orcid.org/0000-0002-1665-7811

References

[1] Evans T.E. *et al* 2004 *Phys. Rev. Lett.* **92** 235003
[2] Bustos A. *et al* 2010 *Nucl. Fusion* **50** 125007
[3] Calvo I. *et al* 2013 *Plasma Phys. Control. Fusion* **55** 125014
[4] Klinger T. *et al* 2017 *Plasma Phys. Control. Fusion* **59** 014018
[5] Kraemer-Flecken A. *et al* 2017 *Nucl. Fusion* **57** 066023
[6] Alejaldre C. *et al* 2001 *Nucl. Fusion* **41** 1449
[7] López-Bruna D. *et al* 2009 *Nucl. Fusion* **49** 085016
[8] Melnikov A.V. *et al* 2017 *Nucl. Fusion* **57** 072004
[9] Pedrosa M.A. *et al* 2008 *Phys. Rev. Lett.* **100** 215003
[10] Sánchez E. *et al* 2013 *Plasma Phys. Control. Fusion* **55** 014015
[11] Cappa A. *et al* 2015 *Nucl. Fusion* **55** 043018
[12] Yoshinuma M. *et al* 2009 *Nucl. Fusion* **49** 062002
[13] McCormick K. *et al* 2002 *Phys. Rev. Lett.* **89** 015001
[14] Velasco J.L. *et al* 2017 *Nucl. Fusion* **57** 016016
[15] Mynick H. 1984 *Phys. Fluids* **27** 2086
[16] García-Regaña J.M. *et al* 2013 *Plasma Phys. Control. Fusion* **55** 074008
[17] Calvo I. *et al* 2017 *Plasma Phys. Control. Fusion* **59** 055014
[18] García-Regaña J.M. *et al* 2017 *Nucl. Fusion* **57** 056004
[19] Ida K. *et al* 2009 *Phys. Plasmas* **16** 056111
[20] Alonso J.A. *et al* 2016 *Plasma Phys. Control. Fusion* **58** 074009
[21] Pedrosa M.A. *et al* 2015 *Nucl. Fusion* **55** 052001
[22] Hidalgo C. *et al* 2016 On the influence of ECRH on neoclassical and anomalous mechanisms using a dual heavy ion beam probe diagnostic in the TJ-II stellarator *Preprint: 2016 IAEA-FEC Conf., (Kyoto, Japan)* EXC/P7-209 (https://conferences.iaea.org/indico/event/98/session/31/contribution/209/material/paper/0.pdf)
[23] Maassberg H. *et al* 1999 *Plasma Phys. Control. Fusion* **41** 1135
[24] Dinklage A. *et al* 2017 The effect of transient density profile shaping on transport in large stellarators and heliotrons *Nucl. Fusion* **57** 066016
[25] McCarthy K. *et al* 2017 *Nucl. Fusion* **57** 056039
[26] Velasco J.L. *et al* 2016 *Plasma Phys. Control. Fusion* **58** 084004
[27] Alonso A. *et al* 2017 *Phys. Rev. Lett.* **118** 185002
[28] Monreal P. *et al* 2016 *Plasma Phys. Control. Fusion* **58** 045018
[29] López-Bruna D., Popov T. and de la Cal E. 2016 *J. Phys.: Conf. Ser.* **700** 012006
[30] de la Cal E. and the TJ-II Team 2016 *Nucl. Fusion* **56** 106031
[31] Tabarés F.L. *et al* 2016 Experimental tests of LiSn alloys as potential liquid metal for the divertor target in a fusion reactor *22 PSI Rome 2016, NM&E* in press
[32] Tabarés F.L. *et al* Direct generation of NBI plasmas in TJ-II with lithium coated walls *Stell. News* sn- 144 (http://web.ornl.gov/info/stelnews/pdf/sn144.pdf)
[33] Velasco J.L., Allmaier K., López-Fraguas A., Beidler C.D., Maassberg H., Kernbichler W., Castejón F. and Jiménez J.A. 2011 *Plasma Phys. Control. Fusion* **53** 115014
[34] de Aguilera A.M. *et al* 2015 *Nucl. Fusion* **55** 113014
[35] Castejón F. *et al* 2016 *Plasma Phys. Control. Fusion* **58** 094001
[36] Nazikian R. *et al* 2008 *Phys. Rev. Lett.* **101** 185001
[37] Sun B.J., Ochando M.A. and López-Bruna D. 2016 *Eur. Phys. Lett.* **115** 35001
[38] Sun B.J. *et al* 2016 *Proc. EPS Conf. on Plasma Physics and controlled Fusion* P1.011 (http://ocs.ciemat.es/EPS2016PAP/pdf/P1.011.pdf)
[39] Estrada T. *et al* 2015 *Nucl. Fusion* **55** 063005
[40] van Milligen B. *et al* 2016 *Nucl. Fusion* **56** 016013
[41] Estrada T. *et al* 2016 *Nucl. Fusion* **56** 026011
[42] Estrada T. *et al* 2016 Plasma flow, turbulence and magnetic islands in TJ-II *Preprint: 2016 IAEA-FEC Conf., (Kyoto, Japan)* EXC/P7-45 (https://conferences.iaea.org/indico/event/98/session/31/contribution/336/material/paper/0.pdf)
[43] López-Bruna D. *et al* 2013 *Plasma Phys. Control. Fusion* **55** 015001
[44] van Milligen B., Estrada T., Carreras B., Ascasíbar E., Hidalgo C., Pastor I., Fontdecaba J., Balbín R. and The TJ-II Team 2016 The causal impact of magnetic fluctuations in slow and fast L-H transitions at TJ-II *Phys. Plasmas* **23** 072305
[45] López-Bruna D. *et al* 2016 Confinement modes and magnetic-island driven modes in the TJ-II stellarator *Preprint: 2016 IAEA-FEC Conf., (Kyoto, Japan)* EX/P7-48 (https://conferences.iaea.org/indico/event/98/session/31/contribution/260/material/paper/0.pdf)
[46] Liu B. *et al* 2015 *Nucl. Fusion* **55** 112002
[47] Losada U. *et al* 2016 *Plasma Phys. Control. Fusion* **58** 084005
[48] Jiménez-Gómez R. *et al* 2011 *Nucl. Fusion* **51** 033001
[49] Melnikov A.V. *et al* 2010 *Nucl. Fusion* **50** 084023
[50] Nagaoka K. *et al* 2013 *Nucl. Fusion* **53** 072004
[51] Melnikov A.V. *et al* 2016 *Nucl. Fusion* **56** 112019
[52] Melnikov A.V. *et al* 2014 *Nucl. Fusion* **54** 123002
[53] Melnikov A. *et al* 2016 *Nucl. Fusion* **56** 076001
[54] Cappa Á. *et al* 2014 *Proc. 25th Int. Conf. on Fusion Energy, (San Petersburg, Russia)* EX/P4-46 (www-naweb.iaea.org/napc/physics/FEC/FEC2014/fec2014-preprints/231_EXP446.pdf)
[55] Sun B.J. *et al* 2015 *Nucl. Fusion* **55** 093023